ISSN 0021-3640, JETP Letters, 2008, Vol. 88, No. 3, pp. 183–188. © Pleiades Publishing, Ltd., 2008.
Original Russian Text © V.R. Shaginyan, K.G. Popov, 2008, published in Pis'ma v Zhurnal Éksperimental'noĭ i Teoreticheskoĭ Fiziki, 2008, Vol. 88, No. 3, pp. 214–219.

General Properties of a Magnetic-Field-Induced Landau Fermi Liquid in High-Temperature Superconductors and Heavy Fermion Metals

V. R. Shaginyan[a] and K. G. Popov[b]

[a] *Petersburg Nuclear Physics Institute, Russian Academy of Sciences, Gatchina, 188300 Russia*
e-mail: vrshag@thd.pnpi.spb.ru

[b] *Komi Science Center, Ural Division, Russian Academy of Sciences, Syktyvkar, 167982 Russia*

Received June 23, 2008

It has been shown that the magnetic-field-induced transition from a non-Fermi-liquid state to a Fermi liquid state in the $Tl_2Ba_2CuO_{6+x}$ high-temperature superconductor is similar to a transition observed in heavy fermion metals. This behavior is explained in the theory of the Fermi condensate quantum-phase transition implying the existence of Landau quasiparticles. The Fermi condensate quantum-phase transition can be considered as a universal cause of the strongly correlated behavior observed in various metals and liquids such as high-temperature superconductors, heavy fermion metals, and two-dimensional Fermi systems.

PACS numbers: 71.27.+a, 72.15.Qm, 74.20.Fg, 74.25.Jb

DOI: 10.1134/S0021364008150083

The non-Fermi-liquid (NFL) behavior observed in strongly correlated Fermi systems such as high-temperature superconductors (HTSCs), heavy fermion metals, and quasi-two-dimensional ^{3}He is actively investigated [1–4]. Of particular interest is the transition from the non-Fermi-liquid behavior to the state of the Landau Fermi liquid, which occurs in the magnetic field and is observed in heavy fermion metals [5, 6]. It is assumed that the extraordinary properties and non-Fermi-liquid behavior observed in HTSCs and heavy fermion metals are determined by the Kondo states, as well as by the critical quantum and thermal fluctuations, which destroy quasiparticles and occur near various magnetic quantum-phase transitions [1–4].

Since a quantum-phase transition occurs at temperature $T = 0$, the controlling parameters are the composition, electron (or hole) number density x, pressure, magnetic field B, etc. The critical point of such a phase transition is shifted to the absolute zero temperature by means of the above parameters. The experimental investigations of the properties of the quantum-phase transition and their magnetic critical points are fundamentally important for an understanding of the physical nature of high-temperature superconductivity and the anomalous behavior of heavy fermion metals. Such investigations for high-temperature superconductivity are absent, because the corresponding critical points at low temperatures are in the superconductivity region and the physical properties of the quantum-phase transition are changed by the superconductivity; the destruction of superconductivity requires strong magnetic fields. Recent investigations of the induction of the transition from the non-Fermi-liquid state to the Landau Fermi liquid one in the $Tl_2Ba_2CuO_{6+x}$ HTSC [7] fill the gap in the experiments and make it possible to determine the properties of the quantum-phase transition specifying the unique properties of the HTSP.

In this work, we show that the (B, T) phase diagrams of the HTSCs and heavy fermion metals are the same although their microscopic natures are different. Analysis of the experimental data on the recovery of the Landau Fermi liquid state in the $Tl_2Ba_2CuO_{6+x}$ HTSC [7] shows that the magnetic-field-induced transition from the non-Fermi-liquid state to the Landau Fermi liquid one coincides with a similar transition observed in the heavy fermion metals. This behavior is explained in the theory of the Fermi condensate quantum-phase transition implying the existence of modified Landau quasiparticles whose effective mass depends on the temperature, magnetic field, and other parameters [8–11]. Thus, the Fermi condensate quantum-phase transition can be considered a universal cause of the strongly correlated behavior observed in various metals and liquids. We also predict that the superconducting phase transition in the HTSCs at low temperatures and in magnetic fields becomes a first-order phase transition, and the differential tunneling conductivity, which is an asymmetric function of the voltage at the non-Fermi-liquid behavior, becomes a symmetric function when the Landau Fermi liquid state is recovered.

To avoid difficulties associated with the anisotropy generated by the crystal lattice of solids, its specificity, irregularities, etc., we use a model of the homogeneous heavy electron (fermion) liquid for studying the univer-

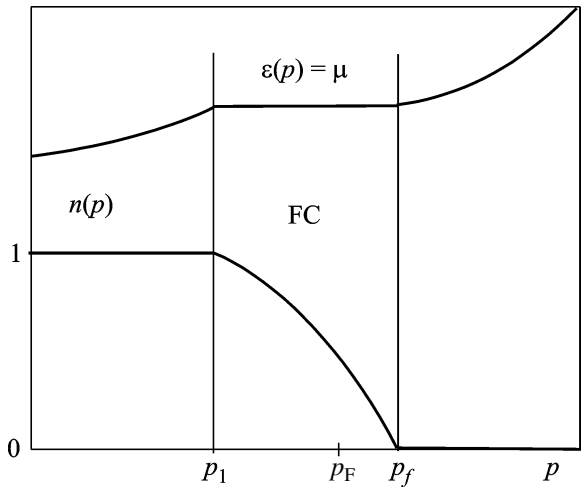

Fig. 1. Distribution function $n(p)$ and single-particle spectrum $\varepsilon(p)$ of the Fermi system with the Fermi condensate. Since $n(p)$ is a solution of Eq. (3), then $0 < n(p_i < p < p_f) < 1$ and $\varepsilon(p_i < p < p_f) = \mu$. The Fermi momentum p_F satisfies the condition $p_i < p_F < p_f$.

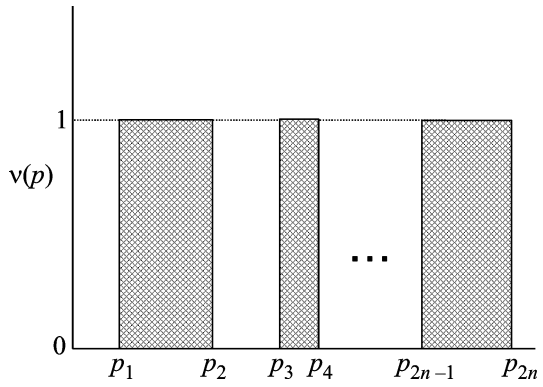

Fig. 2. Function $\nu(p)$ for the multiply-connected distribution changing the function $n(p)$ in the region $p_f - p_i$ filled with the Fermi condensate. The outer Fermi surface at $p \simeq p_{2n} \simeq p_f$ has the form of the Fermi step and the system behaves as the Landau Fermi liquid.

sal behavior of the electron systems of the HTSCs, heavy fermion metals, and quasi-two-dimensional Fermi systems at low temperatures [11].

The effective mass is specified by the known Landau equation [12]

$$\frac{1}{M^*} = \frac{1}{M} + \int \frac{\mathbf{p}_F \mathbf{p}_1}{p_F^3} F(\mathbf{p}_F, \mathbf{p}_1) \frac{\partial n(p_1, T)}{\partial p_1} \frac{d\mathbf{p}_1}{(2\pi)^3}. \quad (1)$$

Here, $F(\mathbf{p}, \mathbf{p}_1)$ is the Landau amplitude, p_F is the Fermi momentum, M is the bare electron mass, and $n(\mathbf{p}, T)$ is the quasiparticle distribution function. The spin dependence is omitted for simplicity. Equation (1) at $T = 0$ provides $M^*/M = 1/(1 - N_0 F^1(x)/3)$, where N_0 is the density of states of a noninteracting electron gas, $x = p_F^3/3\pi^2$ is the density, and $F^1(x)$ is the p component of the Landau amplitude. As a result, M^* diverges at $x = x_c$:

$$\frac{M^*(x)}{M} = \alpha_1 + \frac{\alpha_2}{x_c - x}, \quad (2)$$

where α_1 and α_2 are constants [11]. According to Eq. (2), the effective mass is negative at $x > x_c$. In order to avoid such an unphysical state, the system at the point x_c undergoes the Fermi condensate quantum-phase transition and, forming the Fermi condensate at $x > x_c$, rearranges the topology of the Fermi surface and the distribution function $n(\mathbf{p})$, minimizing the ground-state energy E. For this reason, the distribution function at $x > x_c$ and $T = 0$ is specified by the equation

$$\delta E/\delta n(\mathbf{p}) = \mu, \quad (3)$$

where μ is the chemical potential [8–11, 13, 14]. As a result, the distribution function $n(\mathbf{p})$ becomes smooth near the Fermi momentum p_F, and the Fermi surface transforms to the Fermi volume as seen in Fig. 1. Note that the state with the Fermi condensate is specified by the superconducting order parameter $\kappa(\mathbf{p}) = \sqrt{n(\mathbf{p})(1 - n(\mathbf{p}))}$; therefore, the electron systems with the Fermi condensate and usual pairing interaction are characterized by a superconducting gap $\Delta \propto \lambda$, where λ is the dimensionless magnitude of the pairing interaction. This feature of such systems provides conditions for the formation of a high-temperature superconductivity [8, 9, 11].

The distribution function $n(\mathbf{p})$ in magnetic fields is rearranged. To determine the type of the rearrangement of the state with the Fermi condensate, simple energy reasoning is sufficient. On one hand, the energy benefit ΔE_B due to the destruction of the state with the Fermi condensate is $\Delta E_B \propto B^2$ and approaches zero at $B \longrightarrow 0$. On the other hand, covering a finite interval $p_f - p_i$ in the momentum space, the function $n(\mathbf{p})$ leads to a finite benefit in the ground-state energy as compared to the normal Fermi liquid. A new ground state without a Fermi condensate in weak magnetic fields should have almost the same energy as the state with the Fermi condensate. Such a state is formed by onion-like multiply-connected Fermi spheres, where the smooth function $n(\mathbf{p})$ in the region $p_f - p_i$ is replaced by the distribution $\nu(\mathbf{p})$ with $\kappa(\mathbf{p}) = 0$, which is shown in Fig. 2 [11, 14, 15].

The effective mass $M^*(B)$ in the magnetic field B diverges as $M^*(B) \propto 1/\sqrt{B - B_{c0}}$ [11, 15]. Here, B_{c0} is the critical magnetic field at which a heavy fermion metal is at the quantum critical point tuned by the magnetic field and the corresponding Néel temperature is $T_N(B_{c0}) = 0$. In our simple model of the heavy electron

liquid with the Fermi condensate, B_{c0} is a parameter determined by the specificity of a particular heavy fermion metal. The system with the Fermi condensate placed in the magnetic field $B > B_{c0}$ can return to the Landau Fermi liquid state with $M^*(B)$, which depends on the magnetic field. This means that the dependences $C/T = \gamma_0(B) \propto M^*(B)$ for the specific heat and $\chi(B) \propto M^*(B)$ for the magnetic susceptibility, which are characteristic of the Landau Fermi liquid, are recovered. The quadratic temperature dependence of the resistivity is also recovered: $\rho(T) \propto AT^2$. The coefficient $A(B)$ determines the temperature-dependent resistivity part $\rho(T) = \rho_0 + \Delta\rho$, where ρ_0 is the residual resistivity and $\Delta\rho = A(B)T^2$. Since this coefficient is directly determined by the effective mass [16], $A(B) \propto (M^*(B))^2$,

$$A(B) \simeq A_0 + \frac{D}{B - B_{c0}}, \qquad (4)$$

where A_0 and D are constants. Note that the Kadowaki–Woods empirical relation [17], $K = A/\gamma_0^2 = \text{const}$, is valid in our case [11].

The temperature dependence of $M^*(B, T, x)$ is described by the approximate solution of Landau equation (1):

$$\frac{M^*(B, T_N, x)}{M_M^*} = M_N^*(T_N) \approx c_0 \frac{1 + c_1 T_N^2}{1 + c_2 T_N^{8/3}}. \qquad (5)$$

Here, $M_N^*(T_N)$ is the normalized effective mass, M_M^* is the maximum value of $M^*(B, T, x)$, which is reached at $T = T_{max}$, the normalized temperature T_N is given by the expression $T_N = T/T_{max}$, $c_0 = (1 + c_2)/(1 + c_1)$, and c_1 and c_2 are the constants parameterizing the dipole Landau amplitude and are determined by fitting the experimental data. Equation (5) is consistent with the numerical solutions of Landau equation (1) and determines the universal behavior of the normalized effective mass $M_N^*(T_N)$ of the strongly correlated Fermi liquid in the transition from the Landau Fermi liquid state to the non-Fermi liquid one [11, 18–20]. This behavior is determined by the dimensionless quantities indicated above, because the system near the Fermi condensate quantum-phase transition has no external characteristic scales for measuring T and M^*. According to Eq. (5), M_N^* has three regimes shown in the inset in Fig. 3. The system at $T_N \ll 1$ behaves as the Landau Fermi liquid. At $T_N \sim 1$, the transition regime shown as the shaded region begins: $M_N^*(T_N)$ increases, reaches a maximum $M_N^* = 1$ at $T_N = 1$, and then begins to decrease. The traces of the Landau Fermi liquid disappear at $T_N \gg 1$, when M_N^* decreases first as $T_N^{-2/3}$ and then as $T_N^{-1/2}$.

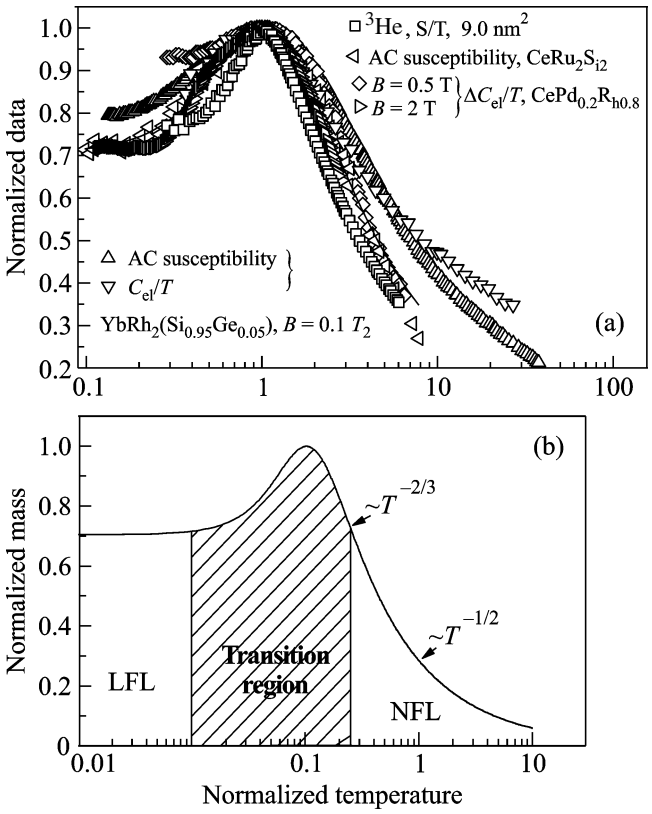

Fig. 3. (a) The normalized mass versus the normalized temperature according to the data extracted from the measurements in the magnetic fields B: the specific heat C and AC magnetic susceptibility on $YbRh_2(Si_{0.95}Ge_{0.05})_2$ [21, 22], susceptibility on $CeRu_2Si_2$ [23], specific heat on $CePd_{1-x}Rh_x$ at $x = 0.80$ [24], and entropy S of two-dimensional ^{3}He at density $x = 9.00$ nm^2 [25]. The solid line is the description by Eq. (5). (b) The universal behavior of the normalized mass. The transition region from the Landau Fermi liquid behavior to the non-Fermi-liquid behavior is shaded.

The magnetic field enters into Eq. (1) through the ratio $\mu_B B/T$; hence, the temperature

$$T^*(B) = a_1 + a_2 B \simeq T_{max} \sim \mu_B(B - B_{c0}) \qquad (6)$$

is the characteristic temperature of the transition from the Landau Fermi liquid state to the non-Fermi-liquid state. Here, a_1 and a_2 are constants and μ_B is the Bohr magnitude. Note that the transition temperature $T^*(B)$ does not specify any phase transition; for this reason, it is associated with a quite wide temperature range shown as the shaded region in Fig. 3b and depends strongly on the determination method. The transition temperature $T^*(B)$ is usually determined from the measurements of the resistivity $\rho(T)$ and corresponds to the point at which the resistivity begins to deviate from the T^2 dependence characteristic of the Landau Fermi liquid.

The experimental values of the normalized effective mass M_N^* are shown in Fig. 3, where the solid line is the

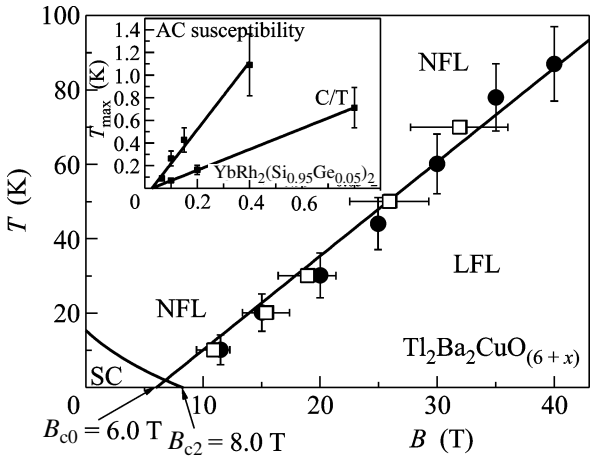

Fig. 4. (B, T) phase diagram of the $Tl_2Ba_2CuO_{6+x}$ HTSC. The measurements of the transition temperature $T^*(B)$ from the Landau Fermi liquid state to the non-Fermi-liquid state [7] are shown by squares and circles, and the straight line is specified by Eq. (6) and separates the Landau Fermi liquid state (LFL) and non-Fermi liquid one (NFL). The arrows in the left corner indicate the critical field $B_{c0} = 6$ T and the critical field $B_{c2} = 8$ T destroying the superconductivity. The region filled with the superconductivity [7] is separated by the solid line and is marked as SC. The inset shows $T_{max} \simeq T^*(B)$; the measurements of the C/T and AC susceptibility were performed on $YbRh_2(Si_{0.95}Ge_{0.05})_2$ [21, 22]. The straight lines plotted according to Eq. (6) intersect at the point $B_{c0} \simeq 0.03$ T.

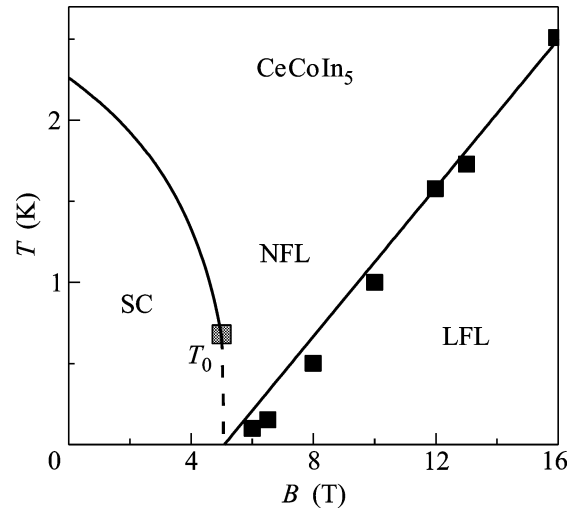

Fig. 5. (B, T) phase diagram of the $CeCoIn_5$ heavy fermion metal. The interface between the superconducting and normal phases is shown by the solid line to the square where the phase transition becomes a first-order phase transition. At $T < T_0$, the phase transition is a first-order phase transition [30]; the interface between the superconducting and normal phases is shown by the dashed line. The solid straight line specified by Eq. (6) with the experimental points [31] shown by squares is the interface between the Landau Fermi liquid (LFL) and non-Fermi-liquid (NFL) states.

approximation by Eq. (5) [19, 20]. According to this figure, Eq. (5) well describes the behavior of the measured effective mass M_N^*; this behavior should be discussed. If the quasiparticles destroyed in the transition region or in the non-Fermi-liquid state, as assumed in various scenarios of the non-Fermi-liquid behavior [1–4], the effective mass M_N^* would be meaningless and would be a function of four variables, rather than exhibit its universal behavior described by function (5). Indeed, M_N^* must depend on T, B, metal-doping level x, and the system density, e.g., the density x of two-dimensional ^{3}He. However, the behavior of the experimental effective mass, which is revealed by means of the above scaling transformations, indicates that the Landau quasiparticles and effective mass are real physical objects in both the Landau Fermi liquid and non-Fermi-liquid states. Only the strong dependence of the effective mass on the normalized temperature, i.e., on the temperature, magnetic field, doping level, system density, and other external parameters is extraordinary.

Figure 4 shows the transition temperature $T^*(B)$ from the Landau Fermi liquid state to the non-Fermi liquid one, which is obtained in the measurements on the $Tl_2Ba_2CuO_{6+x}$ HTSC [7]. The inset shows the temperatures $T_{max} \simeq T^*(B)$ at which the C/T and AC susceptibility have maxima as functions of the magnetic field B. The measurements were performed on the $YbRh_2(Si_{0.95}Ge_{0.05})_2$ heavy fermion metal, which is close to $YbRh_2Si_2$ in properties [21, 22]. Both straight lines shown in the inset at zero temperature pass through the point $B_{c0} \simeq 0.03$ T corresponding to the quantum critical point induced by the magnetic field [21, 22]. The figure shows that all data are described by the linear function of the magnetic field according to Eq. (6).

According to Fig. 4, the critical field $B_{c2} = 8$ T destroying the superconductivity is close to the critical field $B_{c0} = 6$ T at which the metal is at the quantum critical point. This closeness is not accidental, because, as shown above, the state of the system with the Fermi condensate is characterized by the superconducting order parameter $\kappa(\mathbf{p})$and, hence, has a large affinity to the superconductivity [8, 9, 11]. However, as seen in Fig. 2, the Fermi condensate destroys in the magnetic fields $B > B_{c0}$, the system passes to the Landau Fermi liquid state, and the superconducting gap becomes exponentially small at the small coupling constant λ [26], $\Delta \propto \exp - 1/\lambda$, which leads to the destruction of the superconductivity with a further increase in the field. Our consideration shows that $B_{c2} \geq B_{c0}$; i.e., the magnetic quantum critical point is inside or at the edge of the (B, T) region filled with the superconducting phase. Note that, as seen in Fig. 5, $B_{c0} \simeq B_{c2} \simeq 5$ T for $CeCoIn_5$ [6]; the equality $B_{c0} \simeq B_{c2}$ is also valid for

$CeCoIn_{5-x}Sn_x$ at $x \le 0.12$ [27]. However, the equality is invalid in the presence of external pressure, and $B_{c2} > B_{c0}$ for $CeCoIn_5$ [28], which is also valid for other heavy fermion metals, e.g., for $CePd_2Si_2$ [29]. Note that the antiferromagnetic phase in the presence of a weak pairing interaction rejects the superconductivity and $B_{c2} = 0$ as in $YbRh_2Si_2$ and $YbRh_2(Si_{0.95}Ge_{0.05})_2$ metals, which do not transit to the superconducting state at minimum achievable temperatures, and the field B_{c0} is finite [5, 21, 22].

The coincidence of the critical values $B_{c0} \simeq B_{c2}$ leads to the transformation of the superconducting second-order phase transition to the first-order phase transition in magnetic fields close to B_{c2} and at $T < T_0$, as shown in Fig. 5. At relatively high temperatures, when the phase transition is a second-order phase transition, the entropy and other thermodynamic functions are continuous functions at the transition temperature $T_c(B)$. From this continuity condition, we obtain

$$S_{SC}(T \longrightarrow T_c(B)) = S_{NFL}(T \longrightarrow T_c(B)), \qquad (7)$$

where S_{SC} is the entropy of the superconducting phase and S_{NFL} is the entropy of the system in the non-Fermi-liquid state. Since $S_{SC}(T \longrightarrow 0) \longrightarrow 0$ and $S_{NFL}(T \longrightarrow 0)$ approaches the final value S_0 [11], Eq. (7) cannot be satisfied at sufficiently low temperatures $T \le T_0$. Therefore, the second-order phase transition under consideration becomes a first-order phase transition at $T = T_0$, as shown in Fig. 5.

A comparison shows that the (B, T) phase diagrams of $Tl_2Ba_2CuO_{6+x}$ and $CeCoIn_5$ shown in Figs. 4 and 5, respectively, are close to each other; hence, as in $CeCoIn_5$ [11, 32], the superconducting phase transition in the HTSC at low temperatures and in strong magnetic fields can become a first-order phase transition and the differential tunneling conductivity, which is an asymmetric function of the voltage when the system is in the non-Fermi-liquid regime, becomes a symmetric function when the Landau Fermi liquid state is recovered [11, 33]. However, the critical fields for $Tl_2Ba_2CuO_{6+x}$ do not coincide, $B_{c2} > B_{c0}$. For this region, the melt in the fields $B > B_{c2}$ exhibits the Landau Fermi liquid behavior, term S_0 vanishes, and Eq. (7) can be satisfied at sufficiently low temperatures. This circumstance can prevent a change in the transition type.

Figure 6 shows the use of Eq. (4) to approximate the coefficient $A(B)$, which is obtained for (squares) $YbRh_2Si_2$ and (circles) $Tl_2Ba_2CuO_{6+x}$. According to the figure, both sets of the experimental data are well reproduced by Eq. (4), which specifies the universal behavior of $A(B)$ in the Landau Fermi liquid regime. To clearly demonstrate this behavior, we pass to the dimensionless quantities by representing Eq. (4) in the form

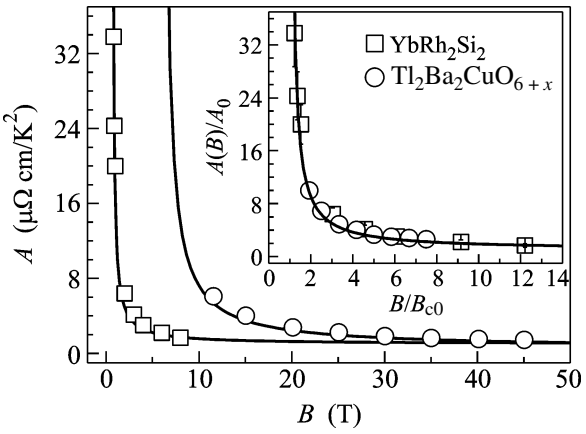

Fig. 6. Coefficient $A(B)$ for (squares) $YbRh_2Si_2$ [5] and (circles) $Tl_2Ba_2CuO_{6+x}$ [7]; the solid lines are the approximations by Eq. (4). The inset shows the normalized coefficient $A(B)/A_0$ versus the normalized magnetic field B/B_{c0}. The solid line is given by Eq. (8) with $A_0 \simeq 0.98$ μΩ cm/K^2.

$$\frac{A(B)}{A_0} \simeq 1 + \frac{D_N}{B/B_{c0} - 1}, \qquad (8)$$

where $D_N = D/A_0B_{c0}$ is the dimensionless constant. According to Eq. (8), the scaling transformation of the description of the coefficient $A(B)$ for the $Tl_2Ba_2CuO_{6+x}$ HTSC and $YbRh_2Si_2$ heavy fermion metal reduces to a function of one variable and one parameter if the corresponding magnetic fields are measured in the units of B_{c0}. For $YbRh_2Si_2$, $B_{c0} \simeq 0.66$ T [5], and $B_{c0} \simeq 6$ T for $Tl_2Ba_2CuO_{6+x}$, as seen in Fig. 4. The inset in Fig. 6 shows the data divided by A_0 for (circles) $Tl_2Ba_2CuO_{6+x}$ and (squares) $YbRh_2Si_2$. The solid line is the approximation by Eq. (8), which indicates that the HTSCs and heavy fermion metals exhibit similar behaviors near the magnetic quantum critical point B_{c0}.

To conclude, we have shown that two different alloys $YbRh_2Si_2$ and $Tl_2Ba_2CuO_{6+x}$, which are characterized by different microscopic properties and belong to different classes of strongly correlated Fermi systems: HTSCs and heavy fermion metals, have the same magnetic quantum critical point associated with the Fermi condensate quantum-phase transition. For this reason, this transition can be considered as a universal cause of the strongly correlated behavior observed in various metals and liquids such as HTSCs, heavy fermion metals, and two-dimensional Fermi systems.

REFERENCES

1. G. R. Stewart, Rev. Mod. Phys. **73**, 797 (2001).
2. P. Coleman and A. J. Schofield, Nature **433**, 226 (2005).

3. H.v. Löhneysen, A. Rosch, M. Vojta, and P. Wölfle, Rev. Mod. Phys. **79**, 1015 (2007).
4. P. Gegenwart, Q. Si, and F. Steglich, Nature Phys. **4**, 186 (2008).
5. P. Gegenwart et al., Phys. Rev. Lett. **89**, 056402 (2002).
6. J. Paglione et al., Phys. Rev. Lett. **91**, 246405 (2003).
7. T. Shibauchi et al., Proc. Natl. Acad. Sci. USA **105**, 7120 (2008).
8. V. A. Khodel and V. R. Shaginjan, Pis'ma Zh. Éksp. Teor. Fiz. **51**, 449 (1990) [JETP Lett. **51**, 507 (1990)].
9. V. A. Khodel, V. R. Shaginyan, and V. V. Khodel, Phys. Rep. **249**, 1 (1994); V. A. Khodel and V. R. Shaginyan, Cond. Mat. Theor. **12**, 222 (1997).
10. G. E. Volovik, Lect. Notes Phys. **718**, 31 (2007).
11. V. R. Shaginjan, M. Ya. Amus'ya, and K. G. Popov, Usp. Fiz. Nauk **177**, 585 (2007) [Phys. Usp. **50**, 563 (2007)].
12. L. D. Landau, Zh. Éksp. Teor. Fiz. **30**, 1058 (1956) [Sov. Phys. JETP **3**, 920 (1956)].
13. V. A. Khodel, Pis'ma Zh. Éksp. Teor. Fiz. **86**, 832 (2007) [JETP Lett. **86**, 721 (2007)].
14. V. A. Khodel, J. W. Clark, and M. V. Zverev, cond-mat/0806.1908.
15. Yu. G. Pogorelov and V. R. Shaginyan, Pis'ma Zh. Éksp. Teor. Fiz. **76**, 614 (2002) [JETP Lett. **76**, 532 (2002)].
16. V. A. Khodel and P. Schuck, Z. Phys. B **104**, 505 (1997).
17. K. Kadowaki and S. B. Woods, Solid State Comm. **58**, 507 (1986).
18. J. W. Clark, V. A. Khodel, and M. V. Zverev, Phys. Rev. B **71**, 012401 (2005).
19. V. R. Shaginyan et al., Phys. Rev. Lett. **100**, 096406 (2008).
20. V. R. Shaginyan, K. G. Popov, and V. A. Stephanovich, Europhys. Lett. **79**, 47001 (2007).
21. J. Custers et al., Nature **424**, 524 (2003).
22. P. Gegenwart et al., Phys. Rev. Lett. **94**, 076402 (2005).
23. D. Takahashi et al., Phys. Rev. B **67**, 180407(R) (2003).
24. A. P. Pikul et al., J. Phys. Condens. Matter **18**, L535 (2006).
25. M. Neumann, J. Nyéki, and J. Saunders, Science **317**, 1356 (2007).
26. J. Bardeen, L. Cooper, and J. R. Shrieffer, Phys. Rev. **108**, 1175 (1957).
27. E. D. Bauer et al., Phys. Rev. Lett. **94**, 047001 (2005).
28. F. Ronning et al., Phys. Rev. B **73**, 064519 (2006).
29. N. D. Mathur et al., Nature (London) **394**, 39 (1998).
30. A. Bianchi et al., Phys. Rev. Lett. **89**, 137002 (2002).
31. J. Paglione et al., Phys. Rev. Lett. **97**, 106606 (2006).
32. V. R. Shaginyan et al., Europhys. Lett. **76**, 898 (2006).
33. V. R. Shaginyan and K. G. Popov, Phys. Lett. A **361**, 406 (2007).

Translated by R. Tyapaev